Received: 24 April 2020 | Revised: 5 August 2020 | Accepted: 12 August 2020

DOI: 10.1002/amp2.10068

RESEARCH ARTICLE

JOURNAL OF ADVANCED MANUFACTURING AND PROCESSING WILEY

# Production and characterization of copper periodic open cellular structures made by 3D printing-replica technique

**Riccardo Balzarotti** | **Alessandra Bisaccia** | **Maria Celeste Tripi** | **Matteo Ambrosetti** | **Gianpiero Groppi** | **Enrico Tronconi**

Dipartimento di Energia, Politecnico di Milano, Milan, Italy

**Correspondence**
Enrico Tronconi, Dipartimento di Energia, Politecnico di Milano, Via La Masa 34, Milano 20156, Italy.
Email: enrico.tronconi@polimi.it

**Funding information**
H2020 European Research Council, Grant/Award Number: Grant Agreement no. 694910/INTENT; Structured Reactors with Intensified Energy Transfer for Breakthrough Catalytic Technologies

**Abstract**

Additive manufacturing by 3D printing comprises a set of methods for production of 3D objects starting from a CAD file. Advantages of additive manufacturing combine high manufacturing resolution, a reduction of waste material, and the possibility of computer-aided design (CAD). When applied to the manufacturing of structured catalyst substrates, the latter enables the optimization of transport properties of the catalyst support. Despite several methods have been introduced for a variety of materials, copper, well known for its high thermal conductivity, is still difficult to be handled. In this work, a novel approach for the additive manufacturing of copper periodic open cellular structures (POCS) is proposed and investigated. It consists in the use of the replica manufacturing procedure starting from resin supports produced by 3D printing stereolithography. Micrometric high purity copper powder was effectively dispersed using a liquid medium based on organic components; the resulting slurry was used for the washcoat deposition on the resin supports. Structures with diamond unit cell shape (cell size of 2.5 mm and void fractions in the 0.8-0.9 range) were washcoated by dip-spin coating. Homogeneous washcoat layers were obtained without occurrence of cell clogging phenomena. Optimized thermal treatment procedure was assessed for sintering the copper POCS. The resulting matrices preserved the morphology of the original structure, reaching a resolution in the range of 70 to 120 μm. These materials can eventually be used as catalyst supports for heat-transfer limited applications (eg, steam reforming of methane), where copper-based substrates were demonstrated to be an effective solution for process intensification.

**KEYWORDS**

3D printing, additive manufacturing, catalyst support, copper, POCS

## 1 | INTRODUCTION

In recent years, a continuous growth of interest in the field of process intensification has been manifest, aiming at fulfilling the increasing demand of more efficient reaction processes.[1] Process intensification is the perfect candidate to fill this gap, as it provides a variety of solutions to improve process productivity, by developing and

adopting cost-effective and multifunctional reactors. In these systems, heat and mass transfer rates can be maximized by the adoption of structured catalyst supports. This is even more important in the case of nonadiabatic processes, as the heat transfer limitations could be more efficiently overtaken by adopting highly conductive metallic structures, thus enabling a faster heat transfer process via the conductive mechanism. The impact of these improvements can be significant when the overall reactor performance is compared to the traditional packed bed configuration.[2]

Metallic structured supports are available in a large variety of forms, such as honeycomb monoliths, open cell foams, felts, and wire meshes.[3] More recently, a novel structured support layout was proposed, which consists in a geometrically well-defined unit cell, which is periodically repeated in the three directions of the space to form a periodic open cellular structure (POCS). Such structures are typically produced by means of additive manufacturing, as this approach allows for a complete tuning and management of the support properties, both in terms of cell size, cell orientation, porosity, strut size, shape and dimension.[4,5] This is one of the major benefits with respect to other cellular supports (ie, open cell foams); in fact, the high design flexibility enables the accurate control of the morphology and the possibility to optimize the structure towards crucial issues of catalyst supports, such as the improvement of heat transfer properties[6] or a better tradeoff between mass transfer and pressure drop.[7] In this view, based on the recent findings of our research group concerning the intensification of the steam reforming process, based on the adoption of conductive packed cellular internals,[8] specifically-designed highly conductive (eg, copper based) POCS could pave the way to a further optimization of the performance of the steam reforming reactor improving the heat transfer and/or the packing efficiency of the internals.

Different techniques are available to 3D print metallic structures,[9] such as robocasting,[10,11] selective electron beam melting (SEBM),[12] selective laser melting (SLM), binder jetting, investment casting[13] and combined 3D printing-replica techniques.

Robocasting enables the deposition of a paste, composed by metal powders or oxides, water and organic compounds by the extrusion through a nozzle: the self-sustaining structures are then heat treated to dry the structure and promote the sintering of metal powders. This method was effectively used for printing copper and stainless steel structures employed for $CO_2$ methanation catalytic applications[10]; however, the methodology provides clear limitations in the geometry of the samples that can be printed.

SEBM and SLM were successfully used for producing metallic supports by means of a high-energy laser beam, which melts/sinters the powder to create a solid structure.[14,15] Among others, copper,[16] aluminum,[17,18] titanium[19] and FeCrAlY supports[20,21] have been printed with this technique. In particular, SEBM was used by Klummp et al. for the production of cubic cell POCS made of Ti-6Al-V4 and the evaluation of pressure drops[19]; structures with different cell sizes, porosities and tilt angle were investigated, using metallic precursor powders with diameters in the range of 45 to 105 μm. The same technique was used by Knorr et al. for the preparation of POCS structures, which were catalytically activated by a carbon supported palladium catalyst for the catalytic hydrogenation of ethane.[22] Structures based on the same bulk material (ie, steel alloy) and produced according to the same preparation technique (ie, SEBM) were tested to investigate mass transfer for gas/liquid applications,[23,24] as well as the heat transfer in liquid flows.[25] While for many materials (ie, Titanium alloy, Stainless steel, Aluminum alloy) the techniques seem industry-ready, in the case of copper clear limitations on the details and the geometries that can be printed are still present.

Binder jetting is a well-established additive manufacturing method that extends the traditional 2D printing process, developing three-dimensional objects. Typically, a liquid binding agent is selectively deposited onto a powder bed: the binder interacts with the particles, thus forming the cross-sectional layer of the object[26]; the excess of powders is then removed and the sample is heat treated for the simultaneous removal of the binder and sintering. Several reviews are available in literature, both focusing on metallic materials (eg, stainless steel,[27] copper[28]) and on ceramic materials.[29]

The use of the techniques introduced so far still represents a challenge for the production of three-dimensional catalytic supports, as the demand for structures with high specific surface area calls for a resolution that is currently the limiting parameter both in terms of dimensional accuracy and small geometries, together with costs and maximum printable size. As an alternative, the manufacturing by conventional investment casting was proposed to overcome some of these limitations, and structures with porosities up to 93% and struts with diameter in the range 0.4 to 1 mm were reported in literature.[13] Moreover, the problem of residual roughness in the range of the dimension of the starting powder, which is a common problem for several other techniques, is prevented thanks to the use of molten metals. Nevertheless, constraints and limitations are still present, both in terms of maximum object dimensions and minimum strut size.

As far as powder-based and layer-by-layer methods are concerned, the aforementioned printing approaches present a variety of critical aspects, which may be summarized in (a) the formation of a molten metal phase and/or (b) the presence of large amounts of powder.

Metal melting may cause severe issues, especially when highly conductive metals are used; in this case, the rapid heat dissipation induces high local thermal gradients that may result in delamination, layer curling, and, in the most severe conditions, part failure.[30] Additionally, if an excess quantity of metal powder is required by the technique, the ductility of the metal and the tendency of powder to agglomerate may impede the post-build powder removal and recovery of the printed parts. Moreover, it should be taken into account that metals in small particles require special handling and storage due to the high sensitivity to oxidation.[31]

In order to overcome many of these limitations, a valuable approach reported in literature consists in the combination of 3D printing and replica techniques: accordingly, first, a polymeric template is produced by additive manufacturing; the use of stereolithography (SLA) can be exploited to produce high-resolution resin structures[32] (with details up to 25 μm and fibers in the range 200-500 μm).

Then, a replica of the polymeric structure is obtained by coating the polymer with a powder slurry of the final desired material and by removing the polymeric template with adequate thermal treatments. This approach represents a good compromise between cost, time and effectiveness, especially when the production of small batches is required.

Despite the promising manufacturing approach, the 3D printing and replica technique was mainly used for the production of ceramic-based supports, such as silicon carbide,[33,34] alumina[35] and zirconium diboride,[36] while most of the aforementioned powder-based methods are only relevant for metallic powders.

Based on this state-of-the-art, the development and assessment of a suitable formulation to be used in the printing and replica technique for the production of metallic POCS were investigated. The experimental investigation was divided into two parts: first, an organic-based formulation was developed and used in a slurry-coating approach to produce copper open cell foams by the replica technique. Then, the methodology was applied and further improved to produce high purity 3D-printed copper POCS. The resin-made lattice structures were produced by SLA. Thus, the new preparation procedure was applied and heat treatment conditions were chosen to obtain 3D objects. The influence of the strut size of the resin backbone was evaluated and a preliminary tuning of the thermal treatment process was carried out. The goal was to set a basis for the investigation of a relatively cheap and easy approach to the manufacturing of POCS metal lattices, especially when small details and/or the use of materials that cannot be printed with additive manufacturing techniques. The declination of these concepts for copper is another novelty factor, which could pave the way to copper periodic open cellular structures to be used as highly conductive reactor internals for nonadiabatic catalytic processes.

## 2 | MATERIALS AND METHODS

### 2.1 | Polymeric precursors of 3D supports

Commercial polyurethane (PU) foams of different cell sizes were used in this study, namely 15 and 25 pore per inch (PPI); samples have been labeled as F15 and F25, in the following (Figure S4A,B). Cell diameter ($d_{cell}$) and strut size ($d_{strut}$) were evaluated with Optical Microscopy and were found to be equal to 4.66 mm and 0.39 mm for the F15 samples and to 3.15 mm and 0.26 mm for the F25 foam, respectively. Void fraction ($\varepsilon_h$) and specific surface area ($S_v$, $cm^{-1}$) were assessed according to a geometrical model of open-cell foams with triangular struts.[37] Based on the cell size and strut diameter, $S_v$ values of 3.9 $cm^{-1}$ and 5.8 $cm^{-1}$ were estimated for the F15 and F25 samples, with a hydraulic void fraction ($\varepsilon_h$) equal to 0.96.

Periodic open cellular structure samples (POCS, cylindric shape, diameter = 9 mm, height = 10 mm) were printed using a Form2 SLA 3D printer, setting a vertical resolution of 25 μm. Samples were produced using a UV-curing resin able to withstand high temperatures (Formlabs High Temp Resin FLHTAM01) with a heat deflection temperature (HDT) of 289°C. SLA exploits the photopolymerization of a liquid resin using a UV-light source. The photo-polymerization enables the formation of a sample anchored to a moving building platform. After printing, structures were first washed in isopropyl alcohol to remove the entrapped liquid medium and then cured using UV light, to improve the mechanical properties. POCS were printed with a diamond cell shape: cell diameter ($d_{cell}$) was held constant at 2.5 mm, while the void fraction was varied between 0.80 and 0.90, by changing the strut size from 530 to 360 μm (Figure S4C–E).

### 2.2 | Slurry preparation and characterization

The slurry was obtained according to a dispersion methodology reported in literature[38,39]; a schematic representation of the procedure is presented in Figure S1. Three different starting solutions, labeled as A, B and C, were separately prepared and then mixed with the metallic powder to obtain the final slurry.

In a typical experiment, formulation A was produced by mixing fish oil (from menhaden, Sigma-Aldrich), xylenes (isomers plus ethylbenzene, Sigma-Aldrich) and ethanol (for residue analysis, Sigma-Aldrich) in a polyethylene jar and keeping them under magnetic stirring for 1 hour. Then, the metallic powder (copper powder, 625 mesh, nominal APS 3.25 to 4.75 μm, 99.9% purity by Alfa Aesar) was added to formulation A: a preliminary slurry was thus obtained and ball milled ($ZrO_2$ grinding bodies, 1 cm diameter, one sphere for each gram of powder) for 18 hours at constant rotation rate (ie, 50 rpm). In the meantime, PVB (polyvinyl butyral, Sigma-Aldrich) and ethanol were mixed in a polyethylene jar and kept under magnetic stirring for 24 hours at low speed, thus obtaining formulation C. After that, formulation B, consisting of PEG (polyethylene glycol 400, Sigma-Aldrich) and BBP (benzyl butyl phthalate, 98%, Sigma-Aldrich), was prepared in a polyethylene jar and kept under stirring for 1 hour. Finally, the ball-milled metallic powder slurry was added to the B + C solution and left under magnetic stirring for 18 hours. All the mixing procedures were performed at room temperature. A summary of slurry compositions is reported in Table S1.

## 2.3 | Coating deposition and consolidation

The aforementioned slurry was deposited onto PU foams using a dip-squeezing coating method: in a typical procedure, the sample was hand-dipped in the copper particles slurry until the whole support was filled by the liquid medium; then the excess slurry was removed by hand squeezing exploiting the elastic behavior of the polyurethane material. Foams were air dried at room temperature for 15 minutes, thus allowing the removal of the volatile part of the formulation (ie, ethanol); samples were weighted after each deposition with the aim of monitoring the washcoat load evolution. This procedure was repeated to determine the increase in washcoat load after each consecutive deposition.

As far as POCS structures are concerned, the metallic coating was deposited using a combination of dip-coating and spin-coating techniques: in a typical procedure, the resin-made sample was first dipped in the slurry and withdrawn by hand; then, a spin coating device (Spin 150i model by SPS Europe) was used in order to remove the excess slurry, thus avoiding the occurrence of clogging phenomena. Spin coating speed, time and acceleration were set at 3500 rpm, 15 seconds and 1500 $rpm \cdot s^{-1}$, respectively. After each deposition, samples were air dried at room temperature for 15 minutes and weighted to monitor the washcoat load evolution. A schematic representation of the methodology used for the washcoat deposition is reported in Figure S2.

After the washcoat deposition process, a proper heat treatment procedure is needed in order to remove the residual organic binders, to decompose the organic matrix and to consolidate the metallic structure. Binders and polymeric structure are removed by a low temperature treatment, at 450°C in air (heating and cooling rate of $5°C \cdot min^{-1}$). Thus, a first tentative thermal treatment temperature was chosen according to two basic considerations: (a) the sintering process occurs below the melting point, (b) the sintering temperature was set higher than 2/3 of the melting temperature, as reported in literature.[40,41] Accordingly, the temperature was set to 900°C for consolidating the copper powder (heating rate of $8°C \cdot min^{-1}$ and overnight cooling).

## 2.4 | Materials characterization

Powder morphology was characterized according to the Brunauer-Emmett-Teller theory (BET porosimetry) and by Hg intrusion measurements by means of Micromeritics ASAP 2020 and MicroActive AutoPore V9600 instrument, respectively. $N_2$ physisorption was not observed and only the inter-particle intrusion was detected, thus excluding the intra-particle one. Thus, powder porosity was considered negligible and not considered in the assessment of the slurry formulation.

Powder particle size distribution was investigated through laser granulometry, using a CILAS 1180 instrument (Compagnie Industrielle des Lasers, Orléans, France).

Slurry rheological properties were assessed by a rotational rheometer set-up with a disc-plate configuration (DSR 200 device by Rheometrics) using a parallel disc geometry (upper plated diameter equal to 40 mm, 0.3 mm gap); viscosity was investigated in the shear rate range between $10^{-1}$ and $10^{3}$ $seconds^{-1}$.

Differential Thermal Analysis-Thermogravimetry (DTA-TG) was performed using a STA7300 instrument (Hitachi). Measurements were carried out in air from room temperature up to 900°C, with a heating rate of $5°C \cdot min^{-1}$.

Washcoat layer homogeneity and morphology were evaluated by optical microscopy, using a SteREO Discovery V12 instrument equipped with an Axiocam ERc 5 seconds camera by Zeiss.

## 3 | RESULTS AND DISCUSSION

### 3.1 | Slurry characterization

A proper slurry dispersion was achieved by means of the ball milling procedure reported in Section 2.2. Given the significant influence of the particle size distribution on the stability of powder dispersions in slurries,[42] powders were evaluated by granulometric analysis before and after the dispersion procedure. Results are presented in Figure 1, where the continuous line indicates the particle size distribution of the copper powder before ball milling (BBM) and dotted line refers to the results after ball milling (ABM).

The pristine powder (BBM) exhibits a monomodal distribution ranging from 1.2 to 11 μm, centered at 10 μm, which evidences a small tail due to the presence of submicronic particles. After the ball milling treatment, a more marked bimodal trend is manifest, with particles smaller than 0.1 μm: here, the two peaks are clearly separated and centered at 0.6 and 6 μm, respectively. Indeed, thanks to the comminution of the biggest particles, a fair number of particles show a diameter included between 0.2 and 1 μm, while the second peak, which appears shifted to the left with respect to BBM, increases in intensity. Accordingly, an overall reduction of the average particle size of copper powder is manifest ABM.

A detailed analysis of the rheological properties of the liquid media was thus performed: measurements were made both for each component of the formulation (A, B and C liquid media, separately) as well as for the slurry of metal powders. Results of the rheological measurements are illustrated in Figure 2.

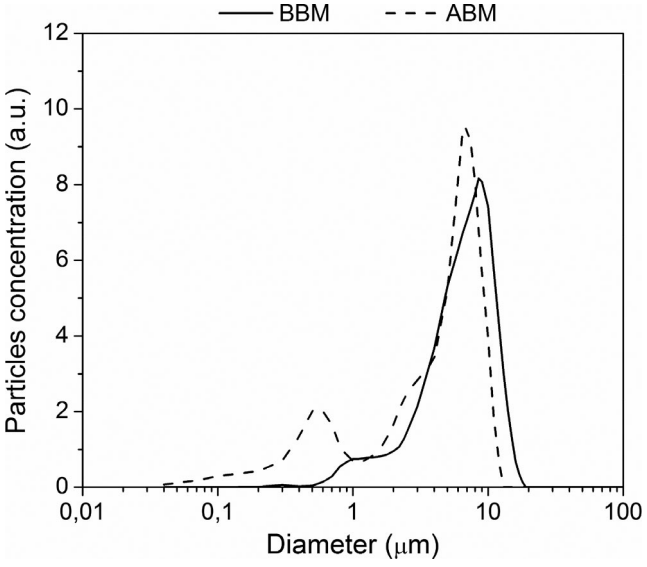


**FIGURE 1** Particle size distribution of the copper powder before ball milling (BBM, continuous lines) and after ball milling (ABM, dotted lines)

Formulation A shows a slightly non-Newtonian behavior, with a decrease in viscosity from 0.01 Pa·s at 0.5 second$^{-1}$ shear rate to 0.006 Pa·s at 1000 seconds$^{-1}$. On the contrary, formulation B displays a more marked shear-thinning behavior up to 1 second$^{-1}$, while the rheologic behavior moves towards a typical Newtonian flow curve at higher shear rates, with a viscosity of 0.07 Pa·s. Concerning formulation C, it follows a non-Newtonian behavior typical of pseudoplastic liquids: the viscosity starts from 450 Pa·s at low shear rate, hence it decreases until 2 Pa·s at the highest shear rate.

The rheological behavior of the three formulations mixed together (ie, the liquid dispersing medium, labeled as ABC in Figure 2B) was also studied, and the results were compared with the metallic copper slurry ABM. According to the results, solution C has a dominant role in determining the final rheological behavior of the dispersing medium (ie, ABC), as the flow curves of the two samples (C and ABC) share many similarities. Nevertheless, a shift towards lower viscosity is evident, likely due to the mixing with less viscous solutions (ie, formulations A and B). As far as the slurry is concerned, the differences in the overall rheological behavior with respect to solution ABC may be ascribed to the presence of liquid - solid interactions. In the 0.1-10 seconds$^{-1}$ shear rate range, a marked non-Newtonian behavior is present, while a fairly constant viscosity of 0.49 Pa·s is approached in the 10-1000 seconds$^{-1}$ shear rate range. The overall rheological behavior is in accordance with previous results reported in literature for the dispersion of micrometric powders in organic-based liquid media,[43] and is suitable for deposition by spin coating technique: according to the previous comments, a viscosity of 0.49 Pa·s was found for shear rate values around 100 seconds$^{-1}$, which is indeed the value of interest for the spin coating process at the selected spin velocities.[44]

### 3.2 | Preliminary investigation of foam production by replica method

Polyurethane foams were used for the preliminary validation of the experimental approach to the production of metallic foams by replica technique, as well as for the evaluation of a proper thermal treatment to consolidate the copper material. As reported in the experimental section, polyurethane foams with different cell sizes (namely 15 and 25 PPI) were used. In order to manage the final washcoat load, multiple depositions were performed, according to the procedure reported in section 2.3. Results are shown in Figure 3.

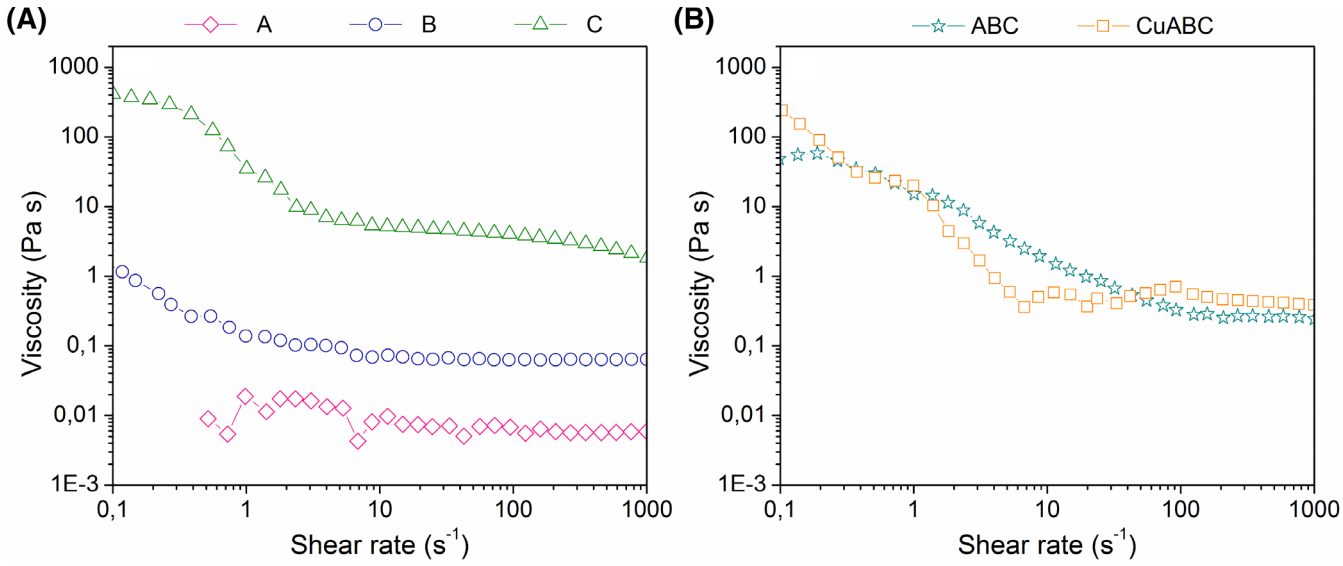


**FIGURE 2** Flow curves of liquid media A, B, and C (A), and rheological behavior of formulation ABC compared with Cu-ABC slurry, (B)

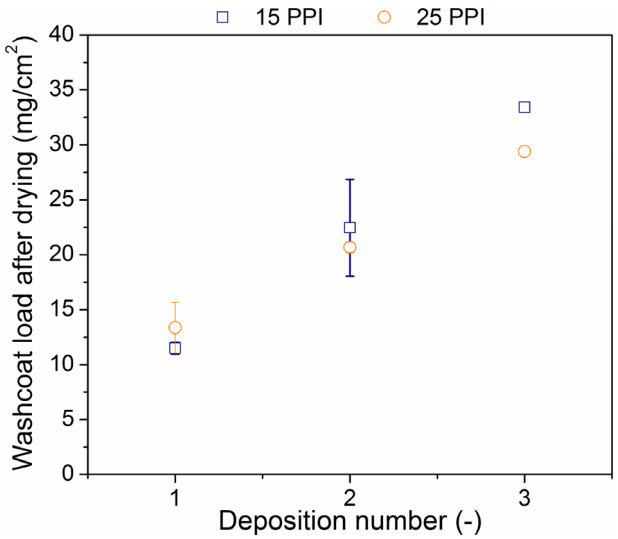


**FIGURE 3** Washcoat load as a function of deposition number for two PU foam samples with different pore density. Error bars are the standard deviations from three replicated samples (one deposition) and two replicated samples (two depositions). Only one samples was produced with three depositions

A linear growth of the washcoat load as a function of the deposition number was found for both the polyurethane open cell substrates. Similar specific loads per unit surface were obtained for the two tested substrates, which correspond to volumetric loads, which increase with the cell density. This aspect may be explained by the fact that an increase in terms of PPI determines an increase in the specific surface area of the support ($S_v$, equal to 3.9 $cm^{-1}$ and 5.8 $cm^{-1}$ for F15 and F25 PPI samples, respectively); thus, a larger surface per unit volume is available for the deposition of the washcoat layer. Taking into consideration the standard deviation (SD) of the data, and in the light of the two abovementioned concurrent phenomena, the two tested samples exhibited a similar behavior in the washcoat formation process.

Washcoated foams were characterized by optical microscopy; results are reported in Figure 4 at different magnifications.

It is evident that a uniform washcoat layer covering the polymeric structure was present in both samples. No pore occlusion was observed for both supports.

Since the aim of this work is the production of metallic substrates, washcoated samples were thermally treated, aiming at: (a) removing the residual organic compounds contained in the washcoat layer, (b) decomposing and removing the polyurethane backbone, and (c) sintering the copper.

Based on these considerations and according to recent results reported in literature for the production of metallic materials,[45] a two-step procedure was selected, as reported in the experimental section: the first heat treatment was performed in air and the second one was carried out in a reducing stream (5% $H_2$, $N_2$ complement).

As far as the in-air stage is concerned, a DTA-TG analysis was carried out in air on the bare polyurethane structure to identify the temperature required to decompose the bare support (Figure S3). A first weight loss was observed in the 200°C range, reaching the total decomposition at 500°C: on the basis of this evidence, a temperature of 450°C was chosen for the first step of the thermal treatment, in order to prevent the total decomposition of the polyurethane matrix, and thus avoid the collapse of the whole structure. The selected temperature was also

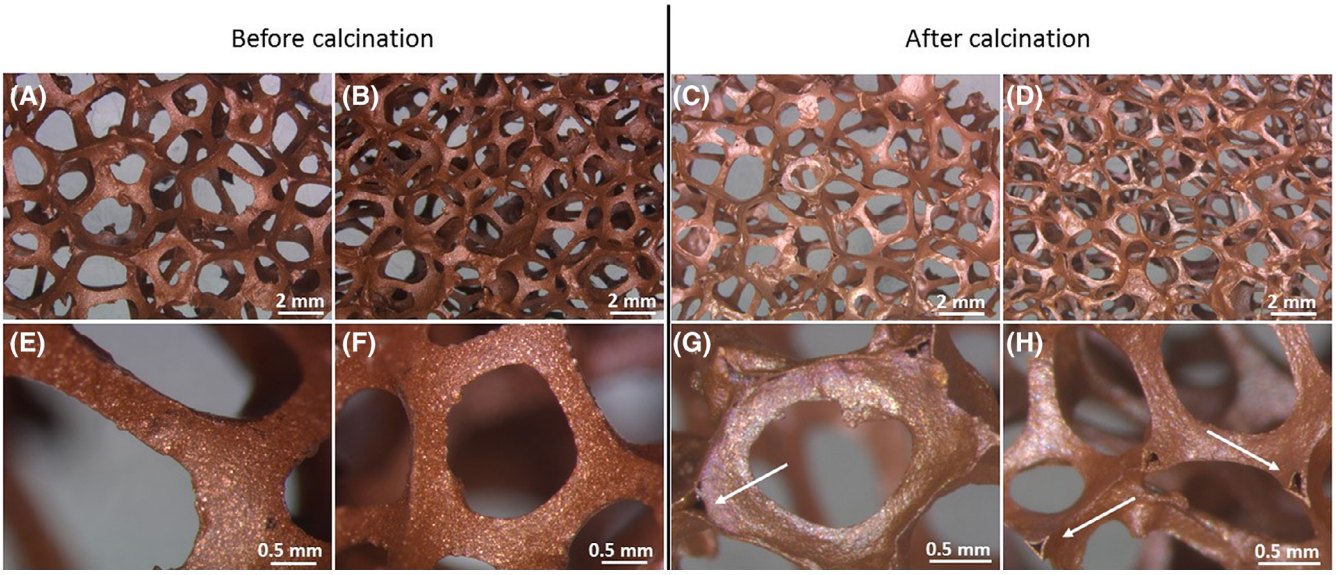


**FIGURE 4** Optical microscope analysis of the washcoated polyurethane supports after three depositions: F15 sample (A,E) and F25 sample (B,F). Results for the metallic sintered supports (three consecutive depositions): 15 PPI foam (C,G) and 25 PPI foam (D,H). Arrows highlight the presence of hollow struts

found to be suitable for the heat treatment of the washcoated structure: taking into account the volatile behavior of the components in the formulation (boiling points between 79 and 450°C), all the organic components of the slurry should be vaporized/decomposed.

The high-temperature sintering in $H_2/N_2$ flow is the second step of the heat treatment procedure. In general, the sintering process allows to compact and form a solid, continuous matrix by varying temperature and pressure without melting the structure. Due to the three-dimensional nature of the object, temperature is the sole parameter that can be tuned to obtain sintered samples. In order to avoid any possible presence of metal oxides, samples were exposed to a reducing atmosphere: the sintering stage was performed in 5% $H_2$ diluted with $N_2$ at 900°C for 4 hours for sintering the copper powder, with a $8°C \cdot min^{-1}$ rate for the heating ramp and overnight cooling. The weight of the samples was monitored before and after the thermal treatment. The obtained metallic structures were further characterized by optical microscopy (Figure 4C,D,G,H).

The selected procedure was applied to the samples produced after three consecutive depositions and it was found to be successful: samples resulted in solid open cell structure, showing good strut homogeneity even at high magnifications. Due to the PU foam decomposition and to the production approach (ie, foam replica method), hollow struts were produced, as evidenced in Figure 4G,H.

By comparing washcoated samples to the resulting metallic foams, a shrinkage phenomenon was observed. This can be due to the superposition of different concurrent phenomena, such as the decomposition of the residual organic binders present in the washcoat layer and the sintering process, which occurs during the high temperature treatment. Gravimetric analysis determined a weight loss of about 40% w/w with respect to the sample weight before thermal treatments, while the average shrinkage of foam diameter was found to be in the 20% range for both samples. The reduction in the volume induced a change in the morphological properties of the open cell foams, reaching a final cell diameter of 3.9 and 2.5 mm for the original F15 and F25 samples, respectively. The reduction in cell diameter and strut size (− 20%) is in the same order of magnitude as the one found for the change of samples volume. A more detailed characterization of the supports is given in Table 1.

The total void fraction ($\varepsilon_{tot}$) of copper foams was calculated according to Equation 1

$$\varepsilon_{tot} = 1 - \frac{V_{Cu}}{V_{foam}}. \quad (1)$$

where $V_{foam}$ ($cm^3$) is the foam total volume and $V_{Cu}$ ($cm^3$) is the volume of copper, calculated as the ratio between the mass of the foam (g) and the copper bulk density ($7.8\ g \cdot cm^{-3}$). During the thermal treatments the polymer is burned out, therefore the final total porosity can significantly differ from that of the original foams. The hydraulic porosity was evaluated on the basis of a previously developed foam geometrical model for foams with triangular struts,[37] using the measured cell and strut

**TABLE 1** Geometric properties of copper foams produced by replica technique

| | Bare foams[a] | | | Cu foams | | | |
|---|---|---|---|---|---|---|---|
| Sample name | $d_{strut}$ (mm) | $d_{cell}$ (mm) | $\varepsilon_h$ | $d_{strut}$ (mm) | $d_{cell}$ (mm) | $\varepsilon_{tot}$ | $\varepsilon_h$ |
| F15 | 0.39 | 4.66 | 0.96 | 0.31 | 3.87 | 0.98 | 0.96 |
| F25 | 0.26 | 3.15 | 0.96 | 0.21 | 2.47 | 0.97 | 0.96 |

[a]The properties of the bare polyurethane foams are also reported as reference.

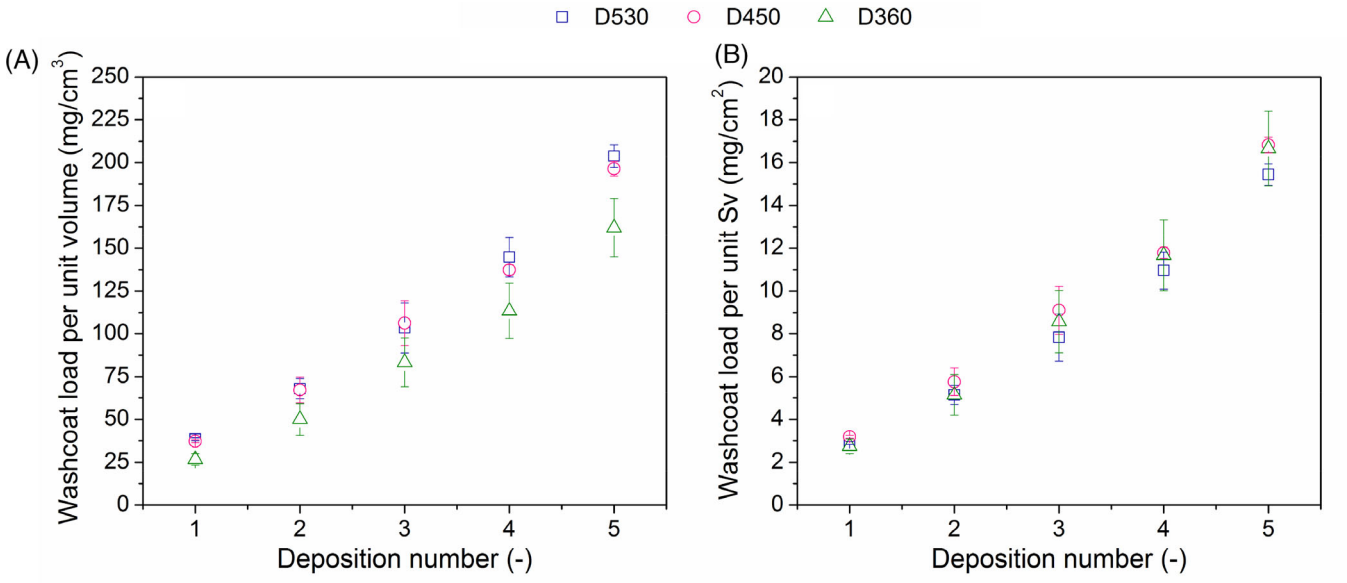


**FIGURE 5** Washcoat load after drying referred to POCS volume (A), and to POCS surface area (B), as a function of deposition number

diameters as input. The difference between total and hydraulic porosity in the case of Cu foams indicate the presence of hollow struts, as clearly shown by Figure 4H.

## 3.3 | Production of copper POCS by 3D printing-replica technique

Due to the promising results obtained for PU foams through the 2-step heat treatment procedure, the same approach was applied to the production of copper POCS via 3D printing-replica method. The diamond cell was selected as the structure of choice: samples were printed at fixed cell size (2.5 mm) and the strut diameter was set at three different values, namely 530, 450, and 360 μm. This resulted in a variation of the void fraction ($\varepsilon$) between 0.8 and 0.9. In the following, samples are named as X-DY, where *X* indicates the metallic powder (Cu), D the unit cell type (diamond) and *X* the strut diameter. Their main specifications are reported in Table S2; cell diameter, POCS diameter, height and, thus, volume were kept constant for all samples. The specific surface area ($S_v$, $cm^{-1}$) was assessed according to the literature.[46]

Coating deposition was performed by dip-spin coating, as described in section 2.3. For each sample, five depositions were performed in order to investigate the evolution of washcoat formation. Results of specific washcoat load after drying (ie, washcoat load referred to the volume and to the specific surface area of the POCS substrate) as a function of the deposition number are presented in Figure 5.

The washcoat load per unit volume increases almost linearly with the number of consecutive depositions, thus enabling a fine control of the process of washcoat growth on POCS supports (Figure 5-a). Samples with smaller strut diameter show a lower loading per unit volume with respect to samples with bigger strut size. At fixed cell size, POCS with smaller strut diameters are characterized by smaller values of $S_v$. Plotting the load in function of the specific surface area shows that, within the experimental error, all the samples follow the same trend, which clearly evidences that the washcoat thickness is

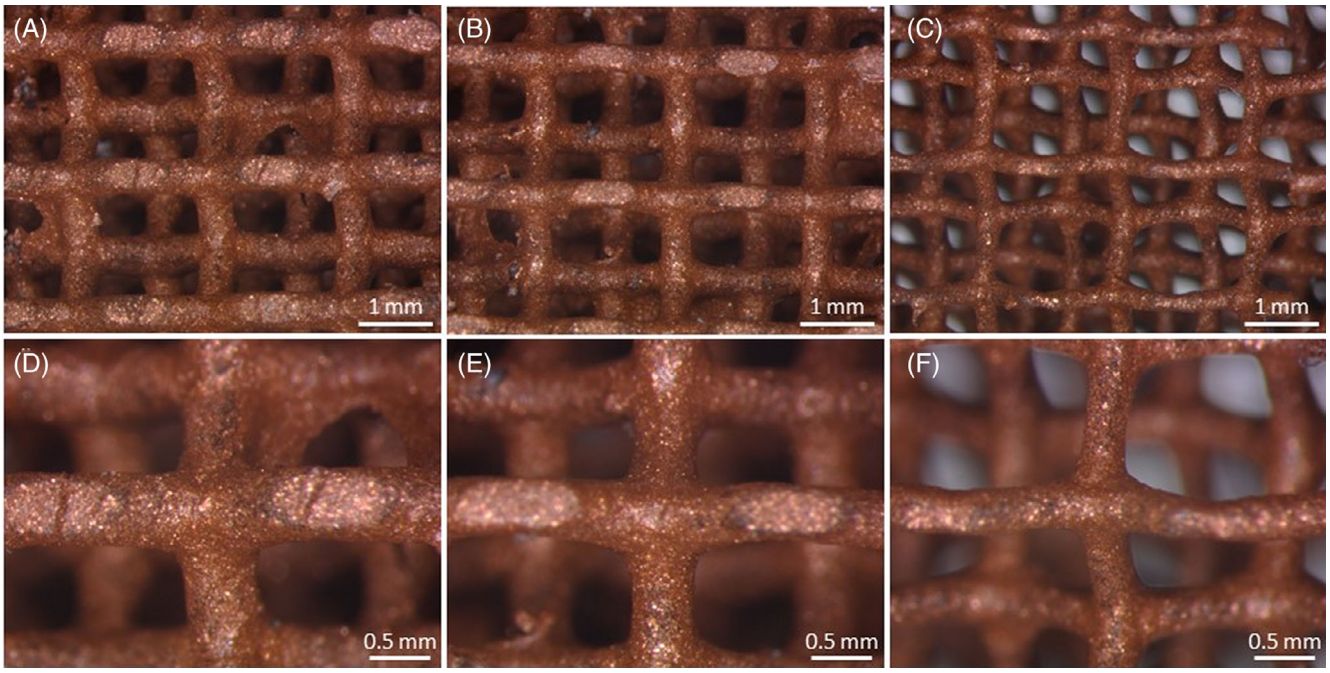


**FIGURE 6** Optical microscope analysis of the washcoated POCS: Cu-D530 (A,D), Cu-D450 (B,E) and Cu-D360 (C,F). Results refer to the samples produced with five consecutive depositions

independent of the strut size and linearly increases with the number of depositions (Figure 5B).

Based on the production of replicated samples, a good reproducibility of the dip-spin coating deposition procedure was achieved. Similarly to the results obtained in Figure 3 for PU foams, also in the case of POCS structures a linear growth of the washcoat load (and thickness) can be noticed with number of depositions. Smaller washcoat loads were found for POCS structures in comparison to open cell foams, likely due to the more effective removal of excess slurry obtained by using the dip-spin coating process.

The copper-coated POCS were characterized by optical microscopy; results are shown in Figure 6 at different magnifications.

After five depositions, an overall homogeneous washcoat layer was found for all the tested structures. The original morphology is preserved, even if minor washcoat accumulations in correspondence of strut junctions was present, probably due to the dynamics of excess slurry removal during the spin-coating process. The optical microscope analyses confirmed that no cell clogging occurred.

Hence, samples were weighted, measured, and subjected to the two-step thermal treatment. The morphological characterization of the calcined samples is given in Figure 7B,C, while the washcoated structure is illustrated in Figure 7A, for comparison. For brevity, only results for the sample Cu-D450 are reported, as the other samples shared the same qualitative properties.

By comparing Figure 7A and Figure 7B, it is clear that the original topology was preserved (ie, diamond cell) after the thermal treatment, despite some deformations are present, likely due to the thermal stresses induced on the structure both during the thermal treatment in air and during the high temperature sintering process. The sintered samples showed a typical metallic-copper aspect, which is a qualitative proof of the thermal treatment effectiveness under $H_2/N_2$ flow. Nevertheless, the presence of localized structural defects can be observed (see magnification in Figure 7C). Such defects are probably due to the lack of optimization of the thermal treatment process. The removal of the resin matrix causes a hollow-strut structure in the metallic POCS, with evident cracks on the strut surface. The final strut shape of POCS structures is affected by more marked homogeneity defects with respect to the results obtained for sintered open cell foams (Figure 4); this may also be attributed to the lower specific washcoat load deposited onto POCS structures, in comparison to foam supports.

In analogy with the open cell foams, shrinkage phenomena occurred during the thermal treatment. By comparing dimensions before and after calcination and sintering, a decrease of about 25% and 30% for the diameter and for the height were detected, respectively. As far as the mass of the samples is concerned, the decrease was found to be higher for samples with thicker struts (ie, lower void fraction). After the heat treatments, weight

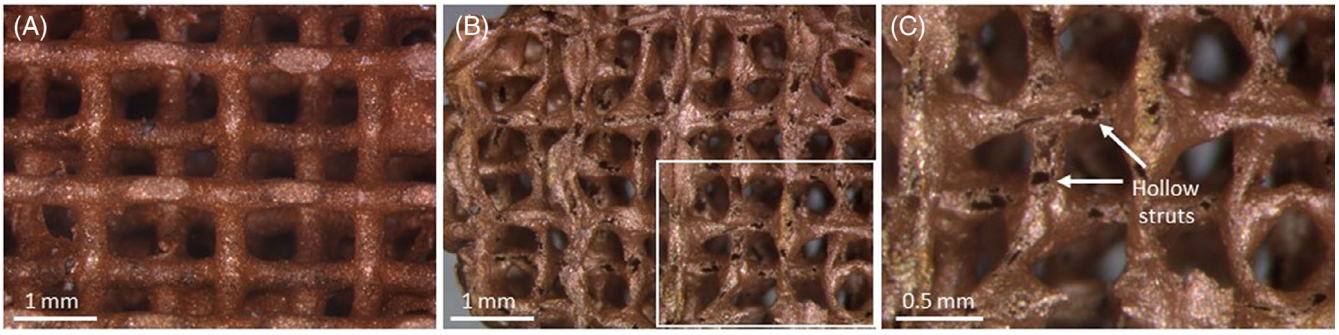


**FIGURE 7** Morphological evolution of Cu-D450 sample before A, and after the two-steps heat treatment (B, and C, at higher magnification)

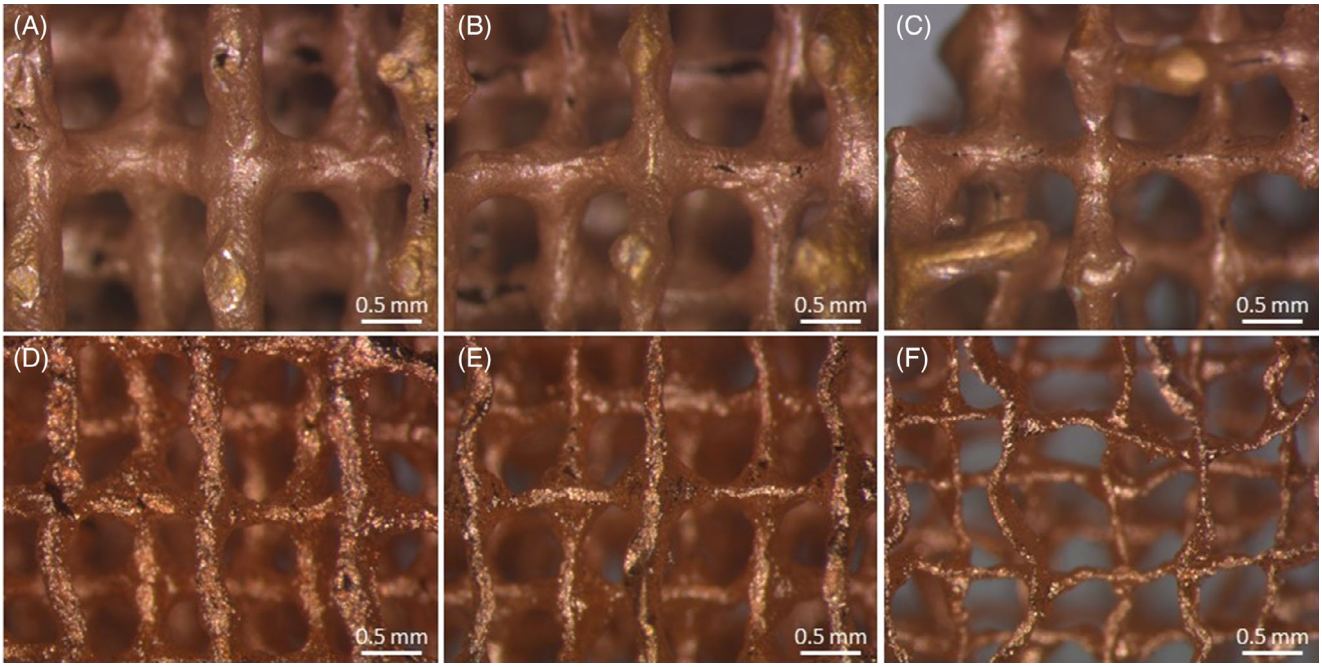


**FIGURE 8** Effect of the different heat treatment procedure on the support morphology: two-steps (first row) and three-steps (second row), tested on Cu-D530 (A,C), Cu-D450 (B,D) and Cu-D360 (C,F). Results refer to the samples produced with 5 consecutive depositions

losses of 63%, 58%, and 47% %wt were found for the Cu-D530, Cu-D450, and Cu-D360 samples, respectively. These values are consistent with the mass of the bare polymeric structures, whose decomposition is responsible for the 84%, 80%, and 69% of the total loss, respectively, and with the mass of binder in the slurry formulation.

## 3.4 | Influence of thermal treatment procedure

The presence of defects on the final POCS metallic structure may be caused by a nonoptimized heat treatment procedure. Accordingly, an alternative procedure based on three thermal treatments (labeled as "three-steps procedure" in the following) was tested: the first steps consisted in heating the samples up to 900°C under a flow of 5% $H_2$ diluted with $N_2$ with a 3°C minutes$^{-1}$ rate for the heating ramp and an overnight natural cooling process. Subsequently, eventual residues of organic precursors were removed by a low temperature treatment, performed at 450°C in air (heating and cooling rate of 5°C·min$^{-1}$). Finally, another step was performed in 5% $H_2$ diluted with $N_2$ at 900°C for 4 hours for reducing and sintering the copper powder, with 8°C·min$^{-1}$ rate for the heating ramp and overnight cooling. The latter two thermal treatments are the same as those carried out in the aforementioned two-steps procedure.

In analogy with the experiments performed using the 2-steps thermal treatment, copper POCS were produced

**TABLE 2** Geometrical properties of the copper POCS produced by 3D printing-replica

| | Bare[a] | | | two-steps treatment | | | | three-steps treatment | | | |
|---|---|---|---|---|---|---|---|---|---|---|---|
| Sample name | $d_{strut}$ (mm) | $d_{cell}$ (mm) | $\varepsilon_{tot}$-$\varepsilon_h$ | $d_{strut}$ (mm) | $d_{cell}$ (mm) | $\varepsilon_{tot}$ | $\varepsilon_h$ | $d_{strut}$ (mm) | $d_{cell}$ (mm) | $\varepsilon_{tot}$ | $\varepsilon_h$ |
| Cu-D530 | 0.53 | 2.5 | 0.80 | 0.35 | 1.84 | 0.96 | 0.84 | 0.12 | 1.35 | 0.94 | 0.96 |
| Cu-D450 | 0.45 | | 0.85 | 0.24 | 1.86 | 0.96 | 0.92 | 0.10 | 1.67 | 0.94 | 0.98 |
| Cu-D360 | 0.36 | | 0.90 | 0.19 | 1.90 | 0.96 | 0.95 | 0.07 | 1.68 | 0.95 | 0.98 |

[a]The properties of the bare supports are also reported as reference.

using the new three step procedure. Results of the characterization by means of the optical microscope are shown in Figure 8D–F for Cu-D530, Cu-D450 and Cu-D360 samples, respectively. The same POCS produced with the two-steps thermal treatment are presented in Figure 8A–C for comparison. Moreover, a qualitative characterization of the evolution of the D530 POCS after each production step is reported in the supplementary material (Figure S5).

A significant change in the morphology was observed for the samples produced with the three-steps procedure: struts were found to be thinner and more compact, resulting in a more uniform material distribution and in the presence of fewer defects on the whole structures, independently from the initial strut size. The new thermal treatment procedure shares the same tendency to copper accumulation at nodes and no pore clogging phenomena were detected. Moreover, it can be noticed that, upon increasing the void fraction, more significant structural deformations occurred (Figure 8F) with respect both to the one obtained after the three-steps treatment (Figure 8C) and to the sample with thicker starting struts (Figure 8D).

In line with the considerations reported so far, samples produced with the three-steps procedure were found to be affected by more severe shrinkage phenomena with respect to those produced with two thermal treatments. In more details, samples showed about 33 and 37% loss in diameter and height, respectively. Furthermore, the weight loss after the thermal treatments was found to follow the same trend and to be similar to the values reported for samples produced with the three-steps treatment: losses equal to 62%, 54% and 48% were found for samples Cu-D530, Cu-D450 and Cu-360, respectively. For a comprehensive view on the manufacturing capabilities herein achieved, a summary of the morphological properties of the POCS samples is reported in Table 2. Bare samples properties were derived from the POCS geometrical model proposed by Lammermann et al.[46] The 3D printed samples with SLA do not display internal porosity; therefore only total porosity was evaluated by sample weighting.

The shrinkage phenomena directly affect the properties of the resulting copper POCS, as in fact a significant reduction of both strut size and cell size was noted. Depending on the starting properties of the resin POCS, remarkably thin struts were produced, ranging from 70 to 120 μm: notably, such values exceed the resolution of most of the current 3D printing solutions used commercially for the additive manufacturing of copper objects. The total porosity of coated samples was evaluated from weight measurements as reported in Equation 1, whereas hydraulic porosity, was calculated from the measurements of $d_{cell}$ and $d_{strut}$ using the geometrical model reported by Lammermann and coworkers[46] and assuming a circular shape of the struts. Very different results are found with the two heat treatment methods. All the samples prepared with the two-step methods exhibit the same total porosity with a consistently lower hydraulic porosity, the difference between $\varepsilon_{tot}$ and $\varepsilon_h$ increasing with the diameter of the strut. The samples prepared with the three-step method show slightly lower total porosity than those based on the two-step one, coherently with the stronger shrinkage. The shrinkage also results in much smaller strut diameter suggesting that internal cavities might have disappeared. A possible explanation of the morphology changes can be found in the different environment conditions of the first thermal treatment step of the two aforementioned methods. At this stage, the sample is composed by (a) the copper powder, (b) the organic binders and, (c) the resin backbone. In the two-steps procedure, the washcoated sample is heated at 450°C in air: in such conditions, the organic components decompose but copper is likely oxidized to copper oxide. Given this operative condition, no sintering can occur, both due to the low temperature and to the presence of copper oxide (which has a higher sintering temperature with respect to metallic copper) and, thus, it is difficult for the washcoat to shrink and to obtain a self-standing defect-free structure. On the contrary, in the three-steps procedure, the first step corresponds to a heat treatment at 900°C under $H_2 + N_2$ stream. In such operative conditions, copper is likely to preserve its metallic phase and, thanks to the high temperature, the washcoat can also undergo the shrinking phenomena, due to the sintering of metallic copper.

However, calculation of the hydraulic porosity leads to inconsistent values, higher than the experimental total

porosity. Such inconsistency can be attributed to strong nonidealities (ie, bending of the struts, deformation of the cross-section, solid accumulation at the nodes), which are evident from Figure 8D–F. Such nonidealities, which are not taken into account in the geometrical model, therefore this can result in inaccurate measurements of $d_{cell}$ and $d_{strut}$ and, consequently in a wrong estimate of the hydraulic porosity. Further experiments are needed for a full rationalization of this aspect.

## 4 | CONCLUSIONS

In this work, the 3D-printing replica procedure was investigated with the aim of producing copper POCS with controlled geometry, such cellular structures being of growing interest as enhanced substrates for the intensification of heat-transfer limited catalytic processes. Technological know-how was achieved by exploring first the production of open-cell copper foams as replica of polyurethane foams. The thus obtained knowledge was effectively transferred to the production of POCS, using the 3D printing-replica method. The most remarkable achievements can be summarized as follows:

- An effective slurry formulation was identified, characterized, and used for the dispersion of micrometric copper powder. The slurry was found to be suitable for washcoat deposition via both dip-squeezing and dip-spin coating techniques.
- A two-steps thermal treatment procedure was validated thanks to the successful production of metallic copper replica foams of the starting polyurethane substrates. Homogeneous struts were obtained, characterized by the typical hollow structure.
- The same methodology was effectively applied to the production of replicated POCS, starting from resin structures produced by additive manufacturing. The methodology was further optimized by adopting a three-steps thermal treatment, which enabled to obtain thinner and more compact struts. With the proposed procedure, it is possible to produce almost defect-free materials with a strut size of 500 μm, that is, better than using state-of-the-art manufacturing techniques. A dedicated experimental campaign focused on the heat treatment process could further elucidate the sintering mechanisms that occur during the consolidation of the samples, and their influence on the properties of the final objects.
- The versatility and robustness of the novel methodology pave the way to the production of POCS using alternative metallic materials (eg, nickel).

## ACKNOWLEDGMENTS

The research leading to these results has received funding from the European Research Council under the European Union's Horizon 2020 Research and Innovation Program (Grant Agreement no. 694910/INTENT: "Structured Reactors with Intensified Energy Transfer for Breakthrough Catalytic Technologies").

## CONFLICT OF INTEREST

The authors declare no conflicts of interest.

## ORCID

*Riccardo Balzarotti* https://orcid.org/0000-0001-5480-0626
*Matteo Ambrosetti* https://orcid.org/0000-0002-5266-2458
*Gianpiero Groppi* https://orcid.org/0000-0001-8099-580X
*Enrico Tronconi* https://orcid.org/0000-0002-5472-2696

## REFERENCES

[1] A. Cybulski, J. A. Moulijn, *Structured Catalysts and Reactors*, 2nd ed. Boca Raton, Florida: CRC Press, **2005**. https://doi.org/10.1201/9781420028003.
[2] E. Tronconi, G. Groppi, C. G. Visconti, *Curr. Opin. Chem. Eng.* **2014**, *5*, 55. https://doi.org/10.1016/j.coche.2014.04.003.
[3] A. Montebelli, C. G. Visconti, G. Groppi, E. Tronconi, C. Cristiani, C. Ferreira, S. Kohler, *Catal. Sci. Technol.* **2014**, *4*, 2846. https://doi.org/10.1039/c4cy00179f.
[4] E. Bianchi, W. Schwieger, H. Freund, *Adv. Eng. Mater.* **2016**, *18*(4), 608. https://doi.org/10.1002/adem.201500356.
[5] A. Inayat, J. Schwerdtfeger, H. Freund, C. Körner, R. F. Singer, W. Schwieger, *Chem. Eng. Sci.* **2011**, *66*(12), 2758. https://doi.org/10.1016/j.ces.2011.03.031.
[6] C. Busse, H. Freund, W. Schwieger, *Chem Eng. Process Process Intensif.* **2018**, *124*(2017), 199. https://doi.org/10.1016/j.cep.2018.01.023.
[7] V. Papetti, P. Dimopoulos Eggenschwiler, A. Della Torre, F. Lucci, A. Ortona, G. Montenegro, *Int. J. Heat Mass Transfer* **2018**, *126*, 1035. https://doi.org/10.1016/j.ijheatmasstransfer.2018.06.061.
[8] R. Balzarotti, M. Ambrosetti, A. Beretta, G. Groppi, E. Tronconi, *Chem. Eng. J.* **2020**, *391*, 123494. https://doi.org/10.1016/J.CEJ.2019.123494.
[9] Y. Zhang, L. Wu, X. Guo, S. Kane, Y. Deng, Y.-G. Jung, J.-H. Lee, J. Zhang, *J. Mater. Eng. Perform.* **2018**, *27*(1), 1. https://doi.org/10.1007/s11665-017-2747-y.
[10] S. Danaci, L. Protasova, F. Snijkers, W. Bouwen, A. Bengaouer, P. Marty, *Chem Eng Process Process Intensif.* **2018**, *127*, 168. https://doi.org/10.1016/j.cep.2018.03.023.
[11] S. Danaci, L. Protasova, J. Lefevere, L. Bedel, R. Guilet, P. Marty, *Catal. Today* **2016**, *273*, 234. https://doi.org/10.1016/j.cattod.2016.04.019.
[12] C. Körner, *Int Mater Rev.* **2016**, *61*(5), 361. https://doi.org/10.1080/09506608.2016.1176289.

[13] A. Anglani, M. Pacella, *Procedia CIRP*. **2018**, *67*, 504. https://doi.org/10.1016/j.procir.2017.12.252.
[14] X. Zhou, C.-J. Liu, *Adv. Funct. Mater.* **2017**, *27*(30), 1701134. https://doi.org/10.1002/adfm.201701134.
[15] C. Parra-Cabrera, C. Achille, S. Kuhn, R. Ameloot, *Chem. Soc. Rev.* **2018**, *47*(1), 209. https://doi.org/10.1039/c7cs00631d.
[16] R. Guschlbauer, S. Momeni, F. Osmanlic, C. Körner, *Mater. Charact.* **2018**, *143*, 163. https://doi.org/10.1016/J.MATCHAR.2018.04.009.
[17] N. F. Bastos Rebelo, K. A. Andreassen, L. I. Suarez Ríos, J. C. Piquero Camblor, H.-J. Zander, C. A. Grande, *Chem. Eng. Process Process Intensif.* **2018**, *127*, 36. https://doi.org/10.1016/J.CEP.2018.03.008.
[18] A. Lind, Ø. Vistad, M. F. Sunding, K. A. Andreassen, J. H. Cavka, C. A. Grande, *Mater. Des.* **2020**, *187*, 1. https://doi.org/10.1016/j.matdes.2019.108377.
[19] M. Klumpp, a. Inayat, J. Schwerdtfeger, C. Körner, R. F. Singer, H. Freund, W. Schwieger, *Chem. Eng. J.* **2014**, *242*, 364. https://doi.org/10.1016/j.cej.2013.12.060.
[20] M. Rombouts, J. P. Kruth, L. Froyen, P. Mercelis, *CIRP Ann.* **2006**, *55*(1), 187. https://doi.org/10.1016/S0007-8506(07)60395-3.
[21] T. Stiegler, K. Meltzer, A. Tremel, M. Baldauf, P. Wasserscheid, J. Albert, *Energy Technol.* **2019**, *7*(6), 1. https://doi.org/10.1002/ente.201900047.
[22] T. Knorr, P. Heinl, J. Schwerdtfeger, C. Körner, R. F. Singer, B. J. M. Etzold, *Chem. Eng. J.* **2012**, *181-182*, 725. https://doi.org/10.1016/j.cej.2011.10.009.
[23] X. Cai, M. Wörner, H. Marschall, O. Deutschmann, *Catal. Today* **2016**, *273*, 151. https://doi.org/10.1016/j.cattod.2016.03.053.
[24] M. Lämmermann, W. Schwieger, H. Freund, *Catal. Today* **2016**, *273*, 161. https://doi.org/10.1016/j.cattod.2016.02.049.
[25] C. Hutter, D. Büchi, V. Zuber, P. Rudolf von Rohr, *Chem. Eng. Sci.* **2011**, *66*(17), 3806. https://doi.org/10.1016/j.ces.2011.05.005.
[26] M. Ziaee, N. B. Crane, *Addit. Manuf.* **2019**, *28*, 781. https://doi.org/10.1016/J.ADDMA.2019.05.031.
[27] S. Mirzababaei, S. Pasebani, *J. Manuf. Mater. Process* **2019**, *3*(3), 82. https://doi.org/10.3390/jmmp3030082.
[28] Y. Bai, C. B. Williams, *Rapid Prototyp. J.* **2015**, *21*(2), 177. https://doi.org/10.1108/RPJ-12-2014-0180.
[29] X. Lv, F. Ye, L. Cheng, S. Fan, Y. Liu, *Ceram. Int.* **2019**, *45*(10), 12609. https://doi.org/10.1016/J.CERAMINT.2019.04.012.
[30] T. I. El-Wardany, Y. She, V. N. Jagdale, J. K. Garofano, J. J. Liou, W. R. Schmidt, *J. Electron. Packag. Trans. ASME.* **2018**, *140*(2), 20907. https://doi.org/10.1115/1.4039974.
[31] T. Q. Tran, A. Chinnappan, J. K. Y. Lee, N. H. Loc, L. T. Tran, G. Wang, V. V. Kumar, W. A. D. M. Jayathilaka, D. Ji, M. Doddamani, S. Ramakrishna, *Metals (Basel).* **2019**, *9*(7), 756. https://doi.org/10.3390/met9070756.
[32] M. Bracconi, M. Ambrosetti, O. Okafor, V. Sans, X. Zhang, X. Ou, C. P. Da Fonte, X. Fan, M. Maestri, G. Groppi, E. Tronconi, *Chem. Eng. J.* **2018**, *377*(October 2018), 120123. https://doi.org/10.1016/j.cej.2018.10.060.
[33] Y. S. Montenegro Camacho, S. Bensaid, S. Lorentzou, N. Vlachos, G. Pantoleontos, A. Konstandopoulos, M. Luneau, F. C. Meunier, N. Guilhaume, Y. Schuurman, E. Werzner, A. Herrmann, F. Rau, H. Krause, E. Rezaei, A. Ortona, S. Gianella, A. Khinsky, M. Antonini, L. Marchisio, F. Vilardo, D. Trimis, D. Fino, *Int. J. Hydrogen Energy* **2017**, *42*(36), 22841. https://doi.org/10.1016/j.ijhydene.2017.07.147.
[34] A. Ortona, C. D'Angelo, S. Gianella, D. Gaia, *Mater. Lett.* **2012**, *80*, 95. https://doi.org/10.1016/J.MATLET.2012.04.050.
[35] A. Herdering, M. Abendroth, P. Gehre, J. Hubálková, C. G. Aneziris, *Ceram. Int.* **2019**, *45*(1), 153. https://doi.org/10.1016/J.CERAMINT.2018.09.146.
[36] M. Aronovici, G. Bianchi, L. Ferrari, M. Barbato, S. Gianella, G. Scocchi, A. Ortona, *J. Am. Ceram. Soc.* **2015**, *98*(8), 2625. https://doi.org/10.1111/jace.13658.
[37] M. Ambrosetti, M. Bracconi, G. Groppi, E. Tronconi, *Chem. Ing. Tech.* **2017**, *89*(7), 915. https://doi.org/10.1002/cite.201600173.
[38] R. E. Mistler, E. R. Twiname, *Tape Casting: Theory and Practice*, Hoboken, New Jersey: John Wiley & Sons, **2006**.
[39] R. K. Nishihora, P. L. Rachadel, M. G. N. Quadri, D. Hotza, *J. Eur. Ceram. Soc.* **2018**, *38*(4), 988. https://doi.org/10.1016/J.JEURCERAMSOC.2017.11.047.
[40] P. S. Liu, G. F. Chen, *Porous Materials* Chapter 2, **2014**, 21. https://doi.org/10.1016/b978-0-12-407788-1.00002-2.
[41] A. Cybulski, J. A. Moulijn, M. M. Sharma, R. A. Sheldon, A. Cybulski, J. A. Moulijn, M. M. Sharma, R. A. Sheldon, *Fine Chem. Manuf.* Chapter 3, **2001**, 59. https://doi.org/10.1016/B978-044482202-4/50003-1.
[42] M. Ambrosetti, R. Balzarotti, C. Cristiani, G. Groppi, E. Tronconi, *Catalysts* **2018**, *8*(11), 510. https://doi.org/10.3390/catal8110510.
[43] R. Balzarotti, L. Fratalocchi, S. Latorrata, E. Finocchio, C. Cristiani, *Appl. Catal A. Gen.* **2019**, *584*, 117089. https://doi.org/10.1016/j.apcata.2019.05.023.
[44] R. Balzarotti, C. Cristiani, L. F. Francis, *Catal. Today* **2019**, *334*(2), 90. https://doi.org/10.1016/j.cattod.2019.01.037.
[45] S. L. Taylor, A. E. Jakus, R. N. Shah, D. C. Dunand, *Adv. Eng. Mater.* **2017**, *19*(11), 1. https://doi.org/10.1002/adem.201600365.
[46] M. Lämmermann, G. Horak, W. Schwieger, H. Freund, *Chem. Eng. Process Process Intensif.* **2018**, *126*(2017), 178. https://doi.org/10.1016/j.cep.2018.02.027.

## SUPPORTING INFORMATION

Additional supporting information may be found online in the Supporting Information section at the end of this article.

**How to cite this article:** Balzarotti R, Bisaccia A, Tripi MC, Ambrosetti M, Groppi G, Tronconi E. Production and characterization of copper periodic open cellular structures made by 3D printing-replica technique. *Journal of Advanced Manufacturing and Processing*. 2020;2:e10068. https://doi.org/10.1002/amp2.10068